PCCP

Accepted Manuscript

ROYAL SOCIETY OF CHEMISTRY

www.rsc.org/pccp

PCCP

RSCPublishing

ARTICLE

Kinetic analysis of the reduction of 4-nitrophenol catalyzed by Au/Pd nanoalloys immobilized in spherical polyelectrolyte brushes

Sasa Gu[1], Yan Lu[1], Julian Kaiser[1], Martin Albrecht[2] and Matthias Ballauff[1,*]

Cite this: DOI: 10.1039/xoxxoooooox

Received ooth January 2012,
Accepted ooth January 2012

DOI: 10.1039/xoxxoooooox

www.rsc.org/

We present a detailed study of the catalytic activity of Au/Pd nanoalloys with Au:Pd molar ratio 75:25 synthesized using spherical polyelectrolyte brushes (SPB) as carrier system. The reduction of 4-nitrophenol (Nip) by sodium borohydride (BH_4^-) has been used as a model reaction. This reaction proceeds in two steps: 4-nitrophenol is first reduced to 4-hydroxylaminophenol which in a second step is reduced to the final product 4-aminophenol. Both steps of the reaction proceed on the surface of the nanoparticles (Langmuir-Hinshelwood-mechanism). We use this model to analyze the experimental data obtained by catalysis with the Au/Pd-nanoalloys. Good agreements between theory and experiments were found up to 30% conversion of Nip. The kinetic parameters were compared with the data derived from neat Au and Pd nanoparticles immobilized in the same SPB carrier system. The addition of 25% molar ratio of Pd to the nanoalloys increases the reaction rate of the first step nearly 10 times compared with that of SPB-Au and 60 times compared with that of SPB-Pd. Analysis of the nanoalloy by high-resolution transmission electron microscopy suggests that the surface defects of the nanoalloys play an important role for the enhanced catalytic activity.

Introduction

Nanoalloys have recently emerged as effective catalysts with physical and chemical properties distinct from individual neat metals[1, 2]. Thus, alloying offers a way to fine-tune the catalytic activity of metallic nanoparticles. In particular, Au/Pd nanoalloys have been widely used as catalysts in organic synthesis[3-5] and advanced photocatalytic processes[6-8] because of the different atomic electron configurations and electronegativities of Pd and Au. Hence, Edwards *et al*[9] used Au/Pd to synthesize of hydrogen peroxide in a direct way while Su *et al*[10] found that Au/Pd supported on TiO_2 exhibits extremely high photocatalytic activity for H_2 production. However, the synergetic effect on catalysis introduced by alloying has not been fully understood in a quantitative manner.

Nanoparticles with diameter of 1~10 nm are usually prepared with surfactants to control the size and prevent aggregation of the nanoparticles during catalysis reactions[11, 12]. However, the surfactants containing alkyl- or thiol- moieties will strongly adsorb on the surface of nanoparticles and may block the catalytic active sites[13]. Recently, spherical polyelectrolyte brushes (SPB) have been successfully used for the immobilization of different metallic nanoparticles and used as "nanoreactors" for catalytic reactions in aqueous solution[14, 15]. The SPB consist of solid colloidal spheres onto which long chains of polyelectrolytes are grafted. The nanoparticles are firmly kept on the surface of the SPB through electrostatic interaction. We could demonstrate that the SPB can be used to prepare well-defined nanoalloy from platinum and gold [16, 17] and from palladium and gold[18].

The catalytic activity of Au/Pd-nanoalloys bound to SPB has recently been studied using the reduction of 4-nitrophenol (Nip) by sodium borohydride (BH_4^-) as a model reaction.[14, 19] This reaction meets all the criterions to evaluate the catalytic activity of nanoparticles:[14] It can be easily monitored by UV-Vis spectroscopy because of the strong absorption of 4-nitrophenolate ions at 400 nm. Moreover, it leads to a single final product without side reactions. Kinetic studies of this reaction have revealed that both reactants must be adsorbed on the surface of the nanoparticles to react (Langmuir-Hinshelwood mechanism)[18-21]. In general, the reduction of Nip adsorbed to the surface of catalytic particles generally follows the so-called direct route:[22-24] Nip is first reduced to 4-nitrosophenol and then quickly to the corresponding 4-hydroxylaminophenol (Hx), which is reduced to 4-aminophenol (Amp) in the rate-determining step. The Hx is therefore the only stable intermediate[24] and the reaction can be treated as two-step reaction as shown in Fig. 1. In all cases studied so far we observe a delay time t_0 after which the reaction starts. There is strong evidence that t_0 is related to a surface-restructuring of the particles necessary to render them catalytically active.[19] Thus, the reduction of 4-nitrophenol catalyzed by metallic nanoparticles seems to be rather well-understood to serve as model reaction.

This reaction has been successfully applied to the analysis of the SPB-Au system.[21] The analysis yields the full information on the kinetics of the scheme shown in Figure 1: First of all, the kinetic constants k_a and k_b are obtained. Moreover, the Langmuir adsorption constants of Nip and Hx are deduced as well. Previously, a simplified version of the kinetic analysis has been developed and applied which takes into account only the stationary state of this reaction.[19, 20] This treatment leads only to the ratio k_b/k_a and not to any further detailed mechanistic information.

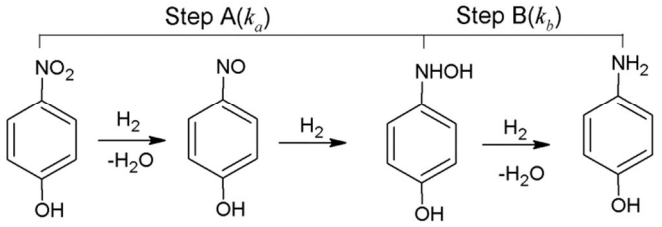

Fig.1 Direct route for the reduction of 4-nitrophenol by metallic nanoparticles: In Step A, 4-nitrophenol (Nip) is first reduced to the 4-nitrosophenol and then converted to 4-hydroxylaminophenol (Hx) quickly, which is the only stable intermediate. In Setp B, Hx is reduced to the final product, namely 4-aminophenol (Amp). Step B is hence the rate-determining step. All reactions take place at the surface of the particles. There is an adsorption/desorption equilibrium for all compounds in all steps.

The analysis of the catalytic activity towards the reduction of Nip using this simplified model has shown that the Au/Pd nanoalloys with Au:Pd molar ratio of 75:25 (denoted as $Au_{75}Pd_{25}$) has the highest activity. Density functional calculations demonstrated that small changes in the atomic arrangement may lead to pronounced alterations of the electronic properties of these particles.[18] Possible reasons for this finding, however, could not be discussed in a quantitative manner.

However, the analysis in ref.[18] has demonstrated that the delay time t_0 could be observed for the Au/Pd nanoalloys as well. This finding points clearly to the strong relation between the surface structure of the Au/Pd nanoalloys and their catalytic activity. More recently, the atomistic structure of the Au/Pd-nanoalloys was analyzed by extended X-ray absorption fine structure analysis (EXAFS).[25] A slight enrichment of Pd-atoms at the surface of the nanoparticles was found. In addition to this, the Pd-atoms located at the surface exhibit a non-metallic character.

These findings prompted us to re-analyze the data given in ref. 18 using the full kinetic scheme[21] shown in Figure 1. The data thus obtained can be compared to the constants obtained from neat Au and neat Pd-nanoparticles. In addition to this, we present an analysis of these nanoalloys by high resolution transmission electron microscopy (HR-TEM) in order to study their surface structure in more detail. This information allows us to elucidate the possible role of surface defects for catalysis[26-29] in further detail for the Au/Pd nanoalloys under consideration here.

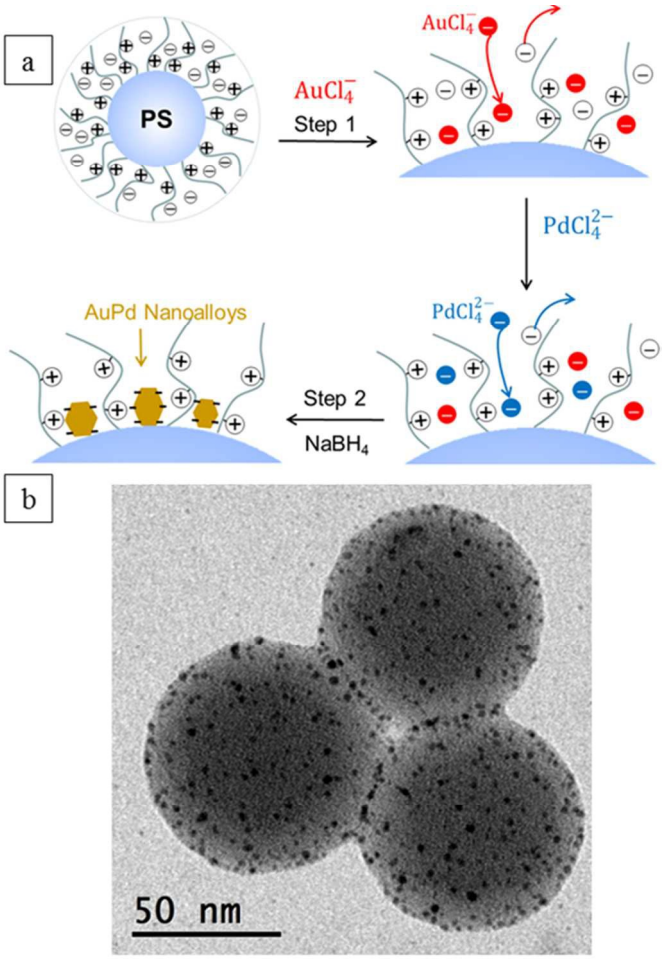

Fig.2 (a) Schematic presentation of the formation of Au/Pd nanoalloys immobilized in the spherical polyelectrolyte brushes (SPB-Au/Pd). Linear cationic poly-(2-aminoethyl methacrylate) (PAEMH) brushes are densely grafted onto a solid polystyrene (PS) core. The chloride counterions are first replaced by $AuCl_4^-$ ions and then by $PdCl_4^{2-}$ ions. Subsequent reduction leads to the formation of nanoalloy particles bound firmly to the surface of the SPB. (b)Representative TEM image of SPB-$Au_{75}Pd_{25}$ (molar ratio Au:Pd=75:25). The dark spots are the Au/Pd nanoparticles with an average size of 2.5 nm.

Experimental

Materials

2-amino-ethylmethacrylate hydrochloride (AEMH, Polyscience, 90%), cetyltrimethylammonium bromide (CTAB, Fluka, 99%), 2,2'-azobis(2-amidinopropane)dihydrochloride (V50, Aldrich, 98%), tetrachloroauric acid trihydrate ($HAuCl_4 \cdot 3H_2O$, Aldrich, 99%), sodium tetrachloropalladate (Na_2PdCl_4, Aldrich, 99%), 4-nitrophenol (Nip, Aldrich, 99%) and sodium borohydride ($NaBH_4$, Aldrich, 98%) were used as received. Styrene (BASF, 99%) was destabilized by Al_2O_3 column and stored in a refrigerator before use. 2-[*p*-(2-Hydroxy-2-methylpropiophenone)]-ethyleneglycol methacrylate (HMEM) was used as the photo-initiator to graft the brushes on the polystyrene cores. The synthesis of this compound has been described previously[30].

Methods

Transmission electron microscopy (TEM) was operated with a JEOL 2100 electron microscope at 200 kV. High resolution-TEM (HR-TEM) was measured by objective lens aberration corrected FEI Titan 80–300 operated at 300 kV. The aberration corrector was set to small negative values < -200 nm.
The amount of metallic nanoparticles immobilized in the SPB was measured by thermogravimetric analysis (TGA) using Netsch STA 409PC LUXX instrument. About 15 mg of dried sample was heated to 800 °C with a heating rate of 10 K/min, and the sample was kept at 800 °C for 1 h. A constant argon flow (30 mL/min) was used during the whole measurement.

Synthesis of Au/Pd nanoalloys immobilized in SPB

SPB with cationic poly(2-amino-ethylmethacrylate hydrochloride) brushes were synthesized as described in ref[15]. SPB supported Au/Pd nanoalloys were prepared as described previously[18]. In brief, the SPB latex solution (100ml, 0.1wt.%) was plugged in N_2 to remove O_2 for 30 min while stirring. Then 5ml solution containing 3.375×10^{-5}mol $HAuCl_4$ and 1.125×10^{-5} mol Na_2PdCl_4 was added to the latex solution. Three-fold of $NaBH_4$ was added drop wise in 30 min to reduce the metal ions. After reaction, the suspension was cleaned in ultrafiltration cell with five-fold excess of water.

Catalytic reduction of 4-nitrophenol

The catalytic reduction of 4-nitrophenol were performed at 20 °C. Generally, the absorption of 4-nitrophenol was monitored by UV-vis spectroscopy using a Lambda 650 spectrometer (Perkin Elmer). The initial concentration of 4-nitrophenol and $NaBH_4$ were changed at different runs, the time depended absorption at 400 nm was collected. Each reaction was repeated three times. The ratio of the concentration c_t of the 4-nitrophenol at time t to its value c_0 at t=0 can be directly determined by the ratio of the respective absorbance A/A_0 at λ = 400 nm from the UV-vis spectrum. The data was averaged and fitted by a MatLab routine as described recently[21].

Results and discussion

Synthesis and characterization

SPB are inert and robust carrier systems for very small nanoparticles, such as Ag[31], Au[32], Pd[33]. In this work SPB with chains of poly (2-aminoethyl methacrylate hydrochloride) (PAEMH) brushes grafted on polystyrene core were used as carrier to generate Au/Pd nanoalloys (see Fig. 2a). The nanoalloys were synthesized in two steps (see Figure 1):[18] $AuCl_4^-$ and $PdCl_4^{2-}$ were firstly introduced into the cationic brushes as counter ions. This mixture of ions localized within the brush layer was reduced by $NaBH_4$ in the second step. In general, nanoparticles synthesized and immobilized in SPB present a unique system inasmuch the entire synthesis of the particles proceeds at ambient temperature, no thermal annealing at elevated temperature is involved. Hence, the nanoalloys under consideration here may present structures far away from equilibrium. Also, all investigations of the catalytic activity reported here are done at room temperature. So we do not expect any major re-arrangement of the internal structure of the nanoparticles as determined recently by EXAFS.[25]

Figure 2b displays the SPB with $Au_{75}Pd_{25}$ nanoparticles that have an average size of 2.5 nm, which are homogeneously distributed on the surface of SPB. In our previous study, it is found that the catalytic activity of nanoalloys with 75% molar ratio of Au and 25% Pd (SPB-$Au_{75}Pd_{25}$) is the highest.[18] To elucidate the reasons for this finding, the catalytic data obtained on the $Au_{75}Pd_{25}$ nanoalloy is analyzed here using the full kinetic scheme shown in Figure 1.

Kinetic model

In the following the essentials of the analysis of the kinetic data in terms of Langmuir-Hinshelwood model will be given.[21] Briefly, three compounds, namely 4-nitrophenol, 4-hydroxylaminophenol and borohydride compete for the active surface sites of nanoalloys. We assume the adsorption and desorption of these three compounds are fast and reversible. The final product 4-aminophenol (Amp) is supposed to desorb from the surface quickly. Thus, it will not appear in the kinetic equations. The surface coverage of Nip, θ_{Nip}, can be modeled in term of Langmuir-Freundlich isotherm:

$$\theta_{Nip} = \frac{(K_{Nip}c_{Nip})^n}{1+(K_{Nip}c_{Nip})^n + K_{Hx}c_{Hx}+K_{BH4}c_{BH4}} \quad (1)$$

Here, K_{Nip}, K_{Hx}, and K_{BH4} are the Langmuir adsorption constants of the respective compounds, and n is the Langmuir-Freundlich exponent. As in ref.[21], n was set as 0.5, the Langmuir-Freundlich exponent for Hx and BH_4 was set as 1. Nip is first reduced to 4-hydroxylaminophenol in Step A, and then further reduced to Amp in Step B. The reaction of Nip can be defined by:

$$-\frac{dc_{Nip}}{dt} = k_{app}c_{Nip} = k_a S\theta_{Nip}\theta_{BH4} = \left(\frac{dc_{Hx}}{dt}\right)_{source} \quad (2)$$

S represents the surface area of used nanoalloys normalized by the volume of reaction solution, which can be calculated by the particle size measured by TEM and the total metal content. k_a is the reaction rate of Step A normalized to S. In the same way the reduction of Hx in Step B can be defined as:

$$-\left(\frac{dc_{Hx}}{dt}\right)_{decay} = k_b S\theta_{Hx}\theta_{BH4} \quad (3)$$

With the Langmuir-Freundlich adsorption isotherm equation, we get[21]

$$-\frac{dc_{Nip}}{dt} = k_a S\frac{(K_{Nip}c_{Nip})^n K_{BH4}c_{BH4}}{\left[1+(K_{Nip}c_{Nip})^n + K_{Hx}c_{Hx}+K_{BH4}c_{BH4}\right]^2} \quad (4)$$

$$\frac{dc_{Hx}}{dt} = k_a S\frac{(K_{Nip}c_{Nip})^n K_{BH4}c_{BH4}}{\left[1+(K_{Nip}c_{Nip})^n + K_{Hx}c_{Hx}+K_{BH4}c_{BH4}\right]^2} - k_b S\frac{K_{Hx}c_{Hx}K_{BH4}c_{BH4}}{\left[1+(K_{Nip}c_{Nip})^n + K_{Hx}c_{Hx}+K_{BH4}c_{BH4}\right]^2} \quad (5)$$

Equation 4 and 5 contain the reaction rates of the different steps as well as the adsorption constants of different components that

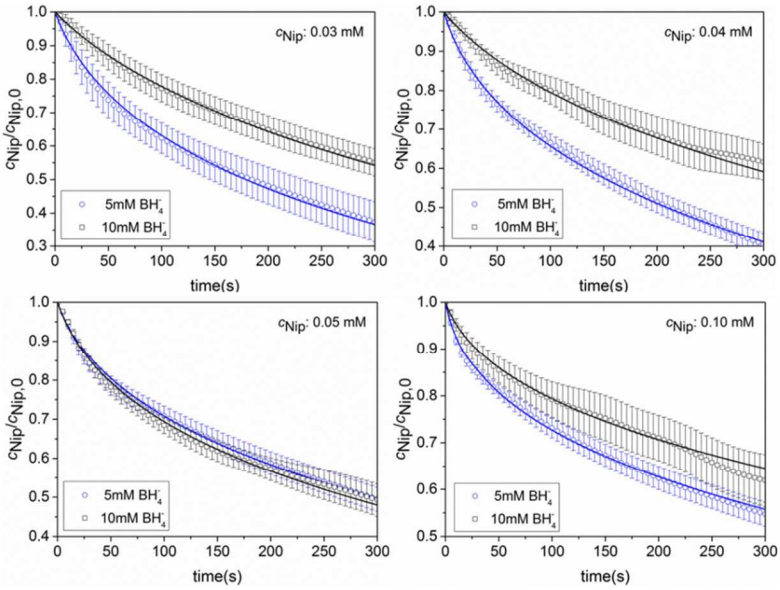

Fig. 3 Fits of the concentration of Nip as the function of time, catalyzed by SPB-$Au_{75}Pd_{25}$ nanoalloys (see the discussion of eq.(4) and (5)). The data have been taken from ref.[18] and induction period of the reaction has been subtracted. The concentration of Nip was normalized to the respective starting concentration $c_{Nip,0}$. The solid lines show the fits. The error bars are merging errors of three parallel experimental data.

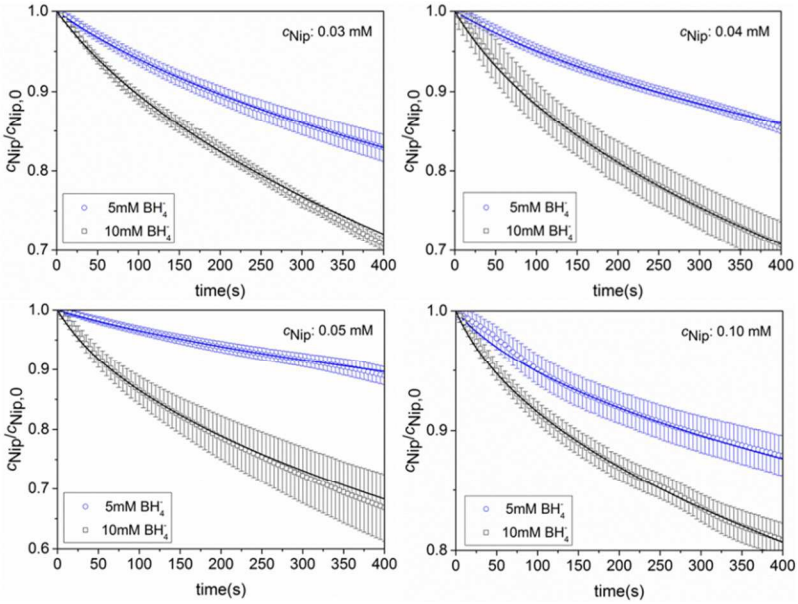

Fig. 4 Fits of the concentration of Nip as the function of time, catalyzed by SPB-Pd nanoparticles (see the discussion of eq.(4) and (5)). The data have been taken from ref.[18] and induction period of the reaction has been subtracted. The concentration of Nip was normalized to the respective starting concentration $c_{Nip,0}$. The solid lines show the fits. The error bars are merging errors of three parallel experimental data.

Table 1 Resulting parameters of the kinetic analysis

parameter	Average k_a [10^{-4}mol/m^2 s]	Average k_b [10^{-5}mol/m^2 s]	K_{Nip} [L/mol]	K_{BH4} [L/mol]	K_{Hx} [L/mol]
SPB-$Au_{75}Pd_{25}$	85.4±23.2	13.4±7.6	3000±800	170±30	(170±20) *10^3
SPB-Au	9.3±2.5[a]	5.1±1.5[a]	3700±900	50±4	(160±15) *10^3
SPB-Pd	1.4±0.4	0.8±0.6	2000±600	70±10	(180±20) *10^3

[a] ref. 21 concentration of Nip no more than 0.1 mM

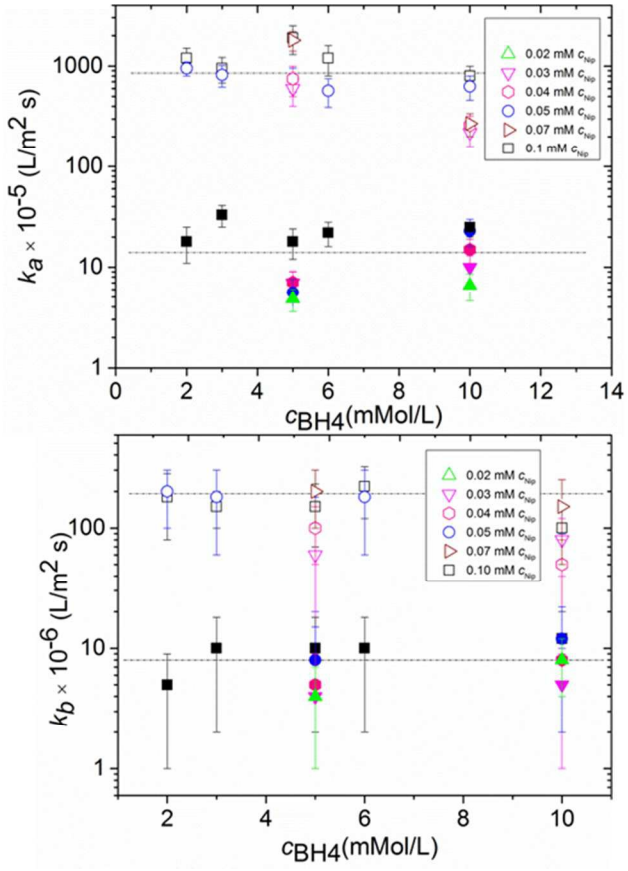

Fig. 5 Kinetic constants k_a and k_b derived from fitting for the reaction catalyzed by SPB-$Au_{75}Pd_{25}$ nanoalloys (hollow points) and SPB-Pd (solid points). The solid points and hollow points with the same shape are at the same Nip concentration as labeled. The dash lines indicate the average value for each set of data. The values within the error bars can fit all corresponding experimental curves.

fully define the kinetics of this reaction. These two equations were used to fit decay of the Nip concentration as described in ref.[21].

Catalytic activity and kinetic analysis

Figure 3 and 4 display the experimental results obtained in ref.[18]. Here the concentration of Nip normalized to the respective initial concentration $c_{Nip,0}$ is shown as the function of time. The induction period of the reaction was subtracted. The data points and the error bars result from averaging experiments of several repeated runs. The solid lines present the fit by the full kinetic model as expressed through eq.(4) and (5). As seen from Fig. 3, the experimental data are well fitted by the kinetic model up to a conversion of Nip of at least 30%. For comparison, SPB-Pd nanoparticles were also used to catalyze the reduction of Nip, as shown in Fig. 4 and S2 in supporting information. The full kinetic model can describe these experimental data well.

All parameters deriving from these fits are listed in Table 1. In both cases, one set of adsorption constants K_{Nip}, K_{BH4} and K_{Hx} is enough to describe all the experiments. The rate constants k_a and k_b are plotted against of the starting concentrations of Nip and BH_4 in Fig. 5. Hollow and solid points are data for $Au_{75}Pd_{25}$ and Pd immobilized in the SPB, respectively. The rate constants are randomly distributed around each average value indicated by dash lines. Since the experiments only measured the decay of Nip, k_b was obtained in an indirect fashion by this analysis. Considering the errors of this analysis, the full kinetic model fits the experimental data very well.

It is clear from Table 1 that the catalytic activity of the SPB-Pd is the smallest. However, the addition of a second species, namely Au, enhances the efficiency of the nanoalloys considerably. A similar finding was also reported for other nanoalloys.[5, 6, 26] In particular, the catalytic activity of SPB-$Au_{75}Pd_{25}$ nanoalloys is much larger than that of SPB-Pd. For the SPB-$Au_{75}Pd_{25}$ nanoalloys, the reaction rate for Step A (see Figure 1), namely k_a, is more than 60 times larger than k_b related to Step B. This difference is much larger compared with the situation of SPB-Au and SPB-Pd as becomes evident when inspecting the data gathered in Table 1. The reduction rate of Nip to 4-hydroxylaminophenol (k_a) catalyzed by nanoalloys is 10 times larger than k_a of SPB-Au and 60 times larger than k_a of SPB-Pd, respectively. The constant k_b related to the reduction of 4-hydroxylaminophenol to Amp, however, is only 2~3 and 15~20 times larger, respectively. Therefore, the catalytic activity for step A is strongly enhanced for the nanoalloy under consideration here. On the other hand, the adsorption constants for the various compounds are of similar magnitude. Hence, the much better catalytic activity of the nanoalloy is mainly due to the acceleration of the surface reduction of Nip in step A, that is, it mainly resides in a much large constant k_a.

Analysis by High-resolution TEM

The surface structure of nanoparticles is one of the most important aspects for their catalytic performance. It is known that molecules generally prefer to adsorb at surface steps since steps may lead to a lower work function and expose available electronic density[34]. For example, Gaspari *et al*[35]. have shown in detail that steps on the Au(111) surface have a pronounced influence on molecular adsorption. Kesavan *et al*[36]. suggested that the catalytic activity can be related to the numbers of surface step/edges in the sample.

In order to elucidate the relationship between catalytic activity and the surface structure of the SPB-$Au_{75}Pd_{25}$ nanoalloy particles in more detail, aberration corrected high- resolution transmission electron microscopy (HR-TEM; Ref.37) was used to analyze the SPB-$Au_{75}Pd_{25}$ composite particles. The central question is the compositional homogeneity and structural perfection of the nanoalloys, in particular for small crystals with a size of 1 to 2 nm only.[38] Previously it has been found that a co- reduction or subsequent reduction of Au(III) and Pd(II) salts in solution normally does not produce single-phase Au-Pd nanoalloy particles and segregation of Pd results.[39] In addition, a core-shell structure often occurs in which a gold core is surrounded by a palladium shell (or vice versa) although Pd and Au are miscible in the macroscopic state.[40, 41]

Fig. 6 displays the HR-TEM images taken for the SPB-$Au_{75}Pd_{25}$ composite particles. It must be noted that the nanoparticles are located directly at the surface where they are kept by electrostatic interaction with the polyelectrolyte chains.[32] The HR-TEM analysis must therefore look for particles located directly at the rims of the core particles. In this way quasi-free particles can be visualized by avoiding any background from the core particles. Evidently, the nanoparticles are oriented at random on the surface of the core particles. Hence, the HR-TEM micrographs are giving projections related to all orientations.

As shown in Fig. 6 the crystal lattice can be clearly observed for the Au-Pd nanoalloys which have a face-centered cubic (fcc) crystalline structure. The nanocrystals are truncated octahedra and bound by {111} and {001} facets. Often monoatomic steps are observed on the {111} facets. A number of particles exhibit stacking faults and twins. However, we do not observe multiply twinned particles. From the comparison of image simulations of core-shell particles and random alloy particles with experimental images we find no indications of core-shell structures in the HR-TEM images. The EXAFS analysis of the alloy samples indicated that the SPB-$Au_{75}Pd_{25}$ sample has the structure which is close to a random alloy. In addition, a partially coverage by Pd^{2+} at the surface is suggested by EXAFS for the Au/Pd alloy particles.

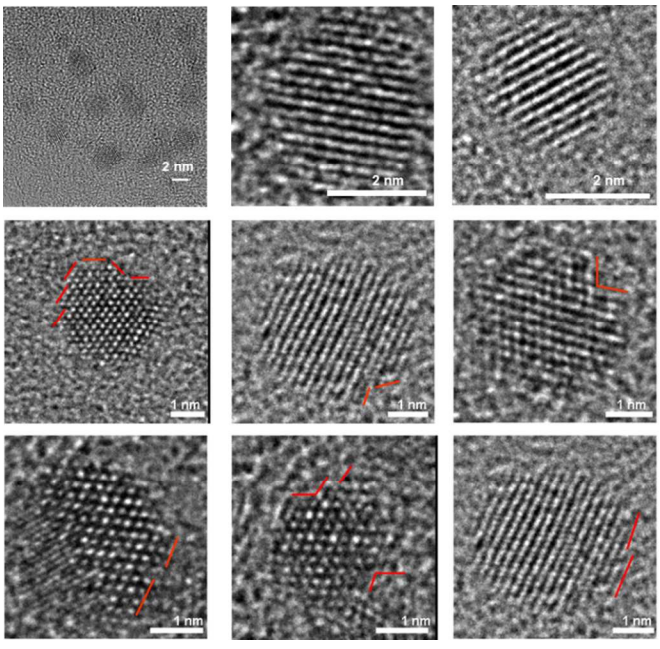

Fig. 6 Representative HR-TEM images for SPB-$Au_{75}Pd_{25}$. Red lines indicate the surface steps of the nanoalloys.

Figure 6 clearly demonstrates that the SPB-$Au_{75}Pd_{25}$ nanoalloys of our study exhibit a large number of surface defects in the HR-TEM images. The atomistic structure of the edges and their defects are clearly visible as indicated by red lines. Evidently, SPB-$Au_{75}Pd_{25}$ nanoalloys are characterized by a large number of surface steps that will contribute to their enhanced catalytic activity. These surface steps may be due to the synthesis by rapid coprecipitation of Au and Pd to form the alloy particles.

Conclusions

We presented a detailed analysis of the catalytic activity of Au/Pd nanoalloys immobilized in spherical polyelectrolyte brushes for the reduction of Nip by BH_4^-. We find that the first step of this reaction, namely the reduction of 4-nitrophenol (see Figure 1) is strongly enhanced. All other parameters as the adsorption constants of the compounds on the surface of the nanoparticles derived from this analysis remain more or less within the range found for neat metal nanoparticles. An analysis of the SPB-$Au_{75}Pd_{25}$ nanoalloy by HR-TEM demonstrated that these nanoparticles exhibit a high number of surface defects. Summarizing these findings and the ones from previous investigations[18, 25] we may state that the better catalytic activity of the SPB-$Au_{75}Pd_{25}$ must be due to

i) electronic effects that lead to a strong enhancement of the constant k_a related to the reaction directly on the surface. This is in line with DFT-calculations[18, 42] pointing to the strong dependence of the electronic properties of the nanoalloys on their composition: The Pd-atoms within the particles lead to a localization of the HOMO mainly located at the surface. However, a part of the Pd-atoms located at the surface exhibit a non-metallic character[25] which is followed by a decrease of catalytic activity as shown here for the case of neat Pd-nanoparticles,

and to ii) the large number of surface defects visible in the HR-TEM micrographs. All this supports the previous conclusion[25] that single Pd-atoms sitting at surface defects constitute the active site of the Au/Pd-nanoalloys. Similar conclusions have been reached for studies of Au/Pd nanoalloys used for reactions in the gas phase.[27, 29]

Acknowledgements

Sasa Gu greatly acknowledges the financial support from China Scholarship Council.

Notes and references

[1] EM-ISFM Institute of Soft Matter and Functional Materials, Helmholtz-Zentrum Berlin für Materialien und Energie, Hahn-Meitner-Platz 1, 14109 Berlin, Germany. Email: Matthias.Ballauff@helmholtz-berlin.de; Fax: +49 (0) 30 8062-43071; Tel: +49 (0) 30 8062-42308

[2] Leibniz-Institut für Kristallzüchtung (IKZ), Max-Born-Strasse 2, 12489 Berlin, Germany

† Electronic Supplementary Information (ESI) available: [Fits of Nip, the value of k_a and k_b from fitting]. See DOI:10.1039/b000000x/

1. I. N. Francesco, F. Fontaine-Vive and S. Antoniotti, *ChemCatChem*, 2014, **6**, 2784-2791.
2. R. Ferrando, J. Jellinek and R. L. Johnston, *Chem. Rev.*, 2008, **108**, 845-910.

3. N. Hayashi, Y. Sakai, H. Tsunoyama and A. Nakajima, *Langmuir*, 2014, **30**, 10539-10547.
4. M. B. Griffin, A. A. Rodriguez, M. M. Montemore, J. R. Monnier, C. T. Williams and J. W. Medlin, *J. Catal.*, 2013, **307**, 111-120.
5. D. Wang, A. Villa, F. Porta, L. Prati and D. Su, *J. Phys. Chem. C*, 2008, **112**, 8617-8622.
6. S. Sarina, H. Zhu, E. Jaatinen, Q. Xiao, H. Liu, J. Jia, C. Chen and J. Zhao, *J. Am. Chem. Soc.*, 2013, **135**, 5793-5801.
7. S. Sarina, S. Bai, Y. Huang, C. Chen, J. Jia, E. Jaatinen, G. A. Ayoko, Z. Bao and H. Zhu, *Green Chem.*, 2014, **16**, 331-341.
8. Q. Xiao, S. Sarina, E. Jaatinen, J. Jia, D. P. Arnold, H. Liu and H. Zhu, *Green Chem.*, 2014, **16**, 4272-4285.
9. J. K. Edwards, J. Pritchard, L. Lu, M. Piccinini, G. Shaw, A. F. Carley, D. J. Morgan, C. J. Kiely and G. J. Hutchings, *Angew. Chem. Int. Ed.*, 2014, **53**, 2381--2384.
10. R. Su, R. Tiruvalam, A. J. Logsdail, Q. He, C. A. Downing, M. T. Jensen, N. Dimitratos, L. Kesavan, P. P. Wells, R. Bechstein, H. H. Jensen, S. Wendt, C. R. A. Catlow, C. J. Kiely, G. J. Hutchings and F. Besenbacher, *ACS Nano*, 2014, **8**, 3490-3497.
11. L. D. Pachon and G. Rothenberg, *Appl. Organomet. Chem.*, 2008, **22**, 288-299.
12. M. Zahmakiran and S. Ozkar, *Nanoscale*, 2011, **3**, 3462-3481.
13. Z. Q. Niu and Y. D. Li, *Chem. Mater.*, 2014, **26**, 72-83.
14. P. Herves, M. Pérez-Lorenzo, L. M. Liz-Marzán, J. Dzubiella, Y. Lu and M. Ballauff, *Chem. Soc. Rev.*, 2012, **41**, 5577-5587.
15. M. Yu, Y. Lu, M. Schrinner, F. Polzer and M. Ballauff, *Macromol. Symp.*, 2007, **254**, 42-45.
16. M. Schrinner, M. Ballauff, Y. Talmon, Y. Kauffmann, J. Thun, M. Möller and J. Breu, *Science*, 2009, **323**, 617-620.
17. M. Schrinner, S. Proch, Y. Mei, R. Kempe, N. Miyajima and M. Ballauff, *Adv. Mater.*, 2008, **20**, 1928--1933.
18. J. Kaiser, L. Leppert, H. Welz, F. Polzer, S. Wunder, N. Wanderka, M. Albrecht, T. Lunkenbein, J. Breu and S. Kümmel, *Phys. Chem. Chem. Phys.*, 2012, **14**, 6487-6495.
19. S. Wunder, Y. Lu, M. Albrecht and M. Ballauff, *ACS Catal.*, 2011, **1**, 908-916.
20. S. Wunder, F. Polzer, Y. Lu, Y. Mei and M. Ballauff, *J. Phys. Chem. C*, 2010, **114**, 8814-8820.
21. S. Gu, S. Wunder, Y. Lu, M. Ballauff, R. Fenger, K. Rademann, B. Jaquet and A. Zaccone, *J. Phys. Chem. C*, 2014, **118**, 18618-18625.
22. H.-U. Blaser, *Science*, 2006, **313**, 312-313.
23. A. Corma and P. Serna, *Science*, 2006, **313**, 332-334.
24. A. Corma, P. Concepción and P. Serna, *Angew. Chem.*, 2007, **119**, 7404-7407.
25. J. Kaiser, W. Szczerba, H. Riesemeier, U. Reinholz, M. Radtke, M. Albrecht, Y. Lu and M. Ballauff, *Faraday Discuss.*, 2013, **162**, 45-55.
26. M. Chen, D. Kumar, C.-W. Yi and D. W. Goodman, *Science*, 2005, **310**, 291-293.
27. J. Xu, T. White, P. Li, C. He, J. Yu, W. Yuan and Y.-F. Han, *J. Am. Chem. Soc.*, 2010, **132**, 10398-10406.
28. C. Ma, Y. Du, J. Feng, X. Cao, J. Yang and D. Li, *J. Catal.*, 2014, **317**, 263-271.
29. J. S. Jirkovský, I. Panas, E. Ahlberg, M. Halasa, S. Romani and D. J. Schiffrin, *J. Am. Chem. Soc.*, 2011, **133**, 19432-19441.
30. X. Guo, A. Weiss and M. Ballauff, *Macromolecules*, 1999, **32**, 6043-6046.
31. Y. Lu, P. Spyra, Y. Mei, M. Ballauff and A. Pich, *Macromol. Chem. Phys.*, 2007, **208**, 254--261.
32. M. Schrinner, F. Polzer, Y. Mei, Y. Lu, B. Haupt, M. Ballauff, A. Göldel, M. Drechsler, J. Preussner and U. Glatzel, *Macromol. Chem. Phys.*, 2007, **208**, 1542-1547.
33. Y. Mei, Y. Lu, F. Polzer, M. Ballauff and M. Drechsler, *Chem. Mater.*, 2007, **19**, 1062-1069.
34. F. Tao and M. Salmeron, *Science*, 2011, **331**, 171-174.
35. R. Gaspari, C. A. Pignedoli, R. Fasel, M. Treier and D. Passerone, *Phys. Rev. B*, 2010, **82**, 041408.
36. L. Kesavan, R. Tiruvalam, M. H. A. Rahim, M. I. bin Saiman, D. I. Enache, R. L. Jenkins, N. Dimitratos, J. A. Lopez-Sanchez, S. H. Taylor, D. W. Knight, C. J. Kiely and G. J. Hutchings, *Science*, 2011, **331**, 195-199.
37. L. C. Gontard, L.-Y. Chang, C. J. D. Hetherington, A. I. Kirkland, D. Ozkaya and R. E. Dunin-Borkowski, *Angew. Chem.*, 2007, **119**, 3757--3759.
38. S. J. Mejía-Rosales, C. Fernández-Navarro, E. Pérez-Tijerina, D. A. Blom, L. F. Allard and M. José-Yacamán, *J. Phys. Chem. C*, 2006, **111**, 1256-1260.
39. L. Prati, A. Villa, F. Porta, D. Wang and D. Su, *Catal. Today*, 2007, **122**, 386-390.
40. T. B. Massalski, H. Okamoto, P. Subramanian and L. Kacprzak, *Binary alloy phase diagrams*, ASM international, 1990.
41. M. R. Knecht, M. G. Weir, A. I. Frenkel and R. M. Crooks, *Chem. Mater.*, 2007, **20**, 1019-1028.
42. G. Zanti and D. Peeters, *J. Phys. Chem. A*, 2010, **114**, 10345-10356.

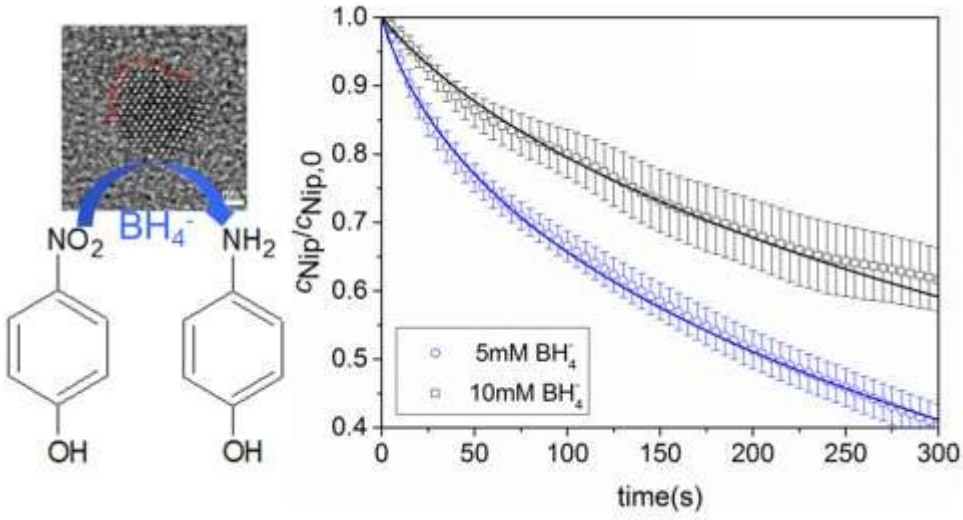

166x94mm (150 x 150 DPI)